INTRSECT: single-component targeting of cells using multiple-feature Boolean logic

Lief E. Fenno[1,2], **Joanna Mattis**[1,2], **Charu Ramakrishnan**[2], **Minsuk Hyun**[2], **Soo Yeun Lee**[2,3], **Miao He**[4], **Jason Tucciarone**[4,5], **Aslihan Selimbeyoglu**[1], **Andre Berndt**[2], **Logan Grosenick**[1,2,3], **Kelly A. Zalocusky**[1,3], **Hannah Bernstein**[6], **Haley Swanson**[3], **Chelsey Perry**[3], **Ilka Diester**[2,7], **Frederick M. Boyce**[8], **Caroline E. Bass**[9], **Rachael Neve**[10], **Z. Josh Huang**[4], and **Karl Deisseroth**[2,3,11,12]

[1]Department of Neuroscience, Stanford University, Stanford CA 94305, USA

[2]Department of Bioengineering, Stanford University, Stanford CA 94305, USA

[3]CNC Program, Stanford University, Stanford CA 94305, USA

[4]Cold Spring Harbor Laboratory, Cold Spring Harbor, NY 11724, USA

[5]Program in Neuroscience, Stony Brook University, Stony Brook, NY 11790, USA

[6]Department of Neuroscience and Physiology, New York University School of Medicine, New York City, NY 10016, USA

[7]Ernst Struengmann Institute for Neuroscience, Frankfurt am Main, Germany

[8]Department of Neurology, Massachusetts General Hospital, Cambridge, MA 02139, USA

[9]Department of Pharmacology and Toxicology, School of Medicine and Biomedical Sciences, University at Buffalo, Buffalo, NY 14214, USA

[10]Department of Brain and Cognitive Sciences, Massachusetts Institute of Technology, Cambridge, MA 02139, USA

[11]Department of Psychiatry and Behavioral Sciences, Stanford University, Stanford CA 94305, USA

[12]Howard Hughes Medical Institute, Stanford University, Stanford CA 94305, USA

Abstract

To whom correspondence should be addressed: Karl Deisseroth, M.D., Ph.D. Department of Bioengineering, W083 Clark Center, 318 Campus Drive Stanford, CA 94305 Phone: (650) 736-4325 deissero@stanford.edu.

Precisely defining the roles of specific cell types is an intriguing and challenging frontier in the study of intact biological systems, and has stimulated the rapid development of genetically-encoded observation and control tools. However, targeting these tools with adequate specificity remains challenging: most cell types are best defined by the intersection of two or more features such as active promoter elements, location, and connectivity. Here we have combined recombinase tools with engineered introns to achieve expression of genetically-encoded payloads conditional upon multiple cell-type features, using Boolean logical operations all governed by a single versatile vector. We use this approach to target intersectionally-specified populations of inhibitory interneurons in mammalian hippocampus and neurons of the ventral tegmental area defined by both genetic and wiring properties. This flexible and modular approach may expand the application of genetically-encoded interventional and observational tools for intact-systems biology.

Introduction

Understanding how defined cell types contribute to organism function is a central goal in biology, and an acute challenge for neuroscience[1]. Recent development of optically-modulated, genetically-encoded tools for testing necessity and sufficiency of precise activity patterns[2,3] has enabled the causal linkage of neuronal activity to circuit dynamics and behavior, but these tools are only as good as their targetability within intact systems. Cell types[4] defined by gene-expression pattern are targetable via either transgenic or viral approaches. While genetically specific, the transgenic approach (inserting genes into defined loci to recapitulate native expression patterns) requires a new animal strain to be generated for each tool. In contrast, viruses are rapidly adaptable, with flexibility in tool payload and injection location. However, suitable promoter fragments (to drive expression of genetically-encoded tools) must be short, strong, and specific; the viral capsid determines packaging efficiency and limits this strategy[3]. Recent approaches have combined the versatility of viral intervention with fuller genetic-specificity conferred by the native chromosomal environment by pairing recombinase-dependent viruses with recombinase-expressing animal lines[5-10].

While elegant, these approaches define cell types by only a single feature. Moreover, cells identical by one marker may serve different or even oppositional roles in physiology or behavior. Therefore there is strong motivation to enable multiple-feature definition, including multiple genetic as well as wiring features. A versatile viral system for defining cell types based on multiple features[4] with only a single nontoxic virus (such as AAV or lentivirus) would powerfully enhance opportunities arising from development of control and observational tools. Targeting cells based on multiple genetic factors generally requires crossing transgenic animals expressing multiple recombinases with animals that express a gene only after recombinase-dependent excision of multiple STOP cassettes[11]. This method has yielded insights into development, but is less scalable and flexible than a viral approach, and is further complicated by transient developmental promoter activity (triggering expression of recombinases), potentially leading to tool expression in off-target adult populations. Viral delivery in the adult would solve this temporal dilemma, but is limited by viral payload limits[3] and the large size of STOP cassettes. Elegant approaches to logical

gene expression using serine integrases have been described *in vitro*[12], but do not utilize recombinases typically built into transgenic mammals, and promoter manipulation strategies used in this approach can be leaky *in vivo* as we show (below). Another approach splits proteins in two pieces, which are separately expressed; functionality results only in cells expressing both pieces. While some function is generated with bacteriorhodopsin[13], channelrhodopsins are poorly expressed this way[14]; more importantly, construction of such an effector protein-specific targeting approach may not be rapidly adaptable to new tools.

Here, we have created a versatile single-AAV system for selective expression conditional upon multiple cell-type features using Boolean logical operations. We validate specificity and potency of the system (which involves custom-modified intronic sequences and diverse recombinases) by expressing opsins and fluorescent proteins both *in vitro* and *in vivo* within populations defined either positively or negatively by multiple genetic or wiring features. Designed for use with broadly available tools, this system is termed INTRSECT, for INTronic Recombinase Sites Enabling Combinatorial Targeting.

RESULTS

Diversifying the single-recombinase-dependent AAVs

We first sought to expand the DIO (double inverted open-reading-frame) Cre-dependent expression system[5-8] by developing conditional-expression vectors dependent upon additional recombinases. We used a mouse-optimized version of Flp[15] which has been applied extensively in Drosophila[4], and we synthesized a human-codon optimized version of phage-derived Dre[16]. Cre, Flp, and Dre recognize short sequences (*Lox*, *FRT*, and *Rox* sites, respectively) that share a standard structure conferring both identity (sites with different spacer sequences cannot recombine) and directionality (sequence between two sites in the same direction is excised; sequence between sites in opposite directions is inverted; Fig. 1a). The DIO strategy uses both excision and inversion[5-8]. The targeted gene is initially anti-sense relative to the promoter, preventing functional transcription. This inverted sequence is flanked by two pairs of incompatible recognition sites (e.g. *loxP* and *lox2722*); two successive recombination events lock the targeted gene into the forward orientation (Fig. 1b). To create Flp- and Dre-dependent DIOs (fDIO and dDIO), we used two *FRT* sites (*FRT* and *F5*[17]) and since only one *Rox* site was known, we created a novel site (*Rox2*) by modifying the *Rox*[16] spacer (Fig. 1a).

We investigated functionality and specificity of these DIOs *in vitro* using channelrhodopsin (ChR2)-eYFP as a payload. HEK293 cells were transfected with each DIO alone, or also with each recombinase, and analyzed for fluorophore expression using flow cytometry (Fig. 1c,d). To quantify the results, we assessed whether the data was better fit by a single curve (indicating a uniform population of eYFP negative cells) or by multiple curves (indicating mixed eYFP positive and negative cells; see Methods). All DIOs in isolation had expression levels comparable to the negative control. When cotransfected with the correct recombinase, all DIOs had robust expression (Fig. 1d). Notably, Cre and Dre exhibited cross-reactivity (Fig. 1c,d; arrowheads), while Flp and fDIO were independent of cDIO/dDIO and Cre/Dre respectively.

To test *in vivo* functionality, we co-injected viruses encoding each DIO-ChR2-eYFP and each recombinase into mouse hippocampus (Fig. 1e). All DIOs had virtually no leak in isolation and strong expression with the correct recombinase (Fig. 1f,g). Cross-activation was observed *in vivo* between dDIO-ChR2-eYFP and Cre (Supplementary Fig. 1), but not Dre and cDIO-ChR2-eYFP. ChR2 stimulation *in vivo* evoked strong activity in all cases (Fig. 1h).

Development of a Cre AND Flp-dependent construct

With the goal of targeting based on multiple features, we first paired Cre and Flp (chosen for lack of detectable cross-reactivity and for increasingly-available driver lines) to independently control relative directionality of the promoter and open reading frame (ORF; Supplementary Fig. 2a-d; also see[12]), but observed inappropriate expression *in vivo*. The second strategy used nested recombinases to manipulate separate domains of the ORF (Supplementary Fig. 3e-i), but suffered from low expression.

Next, we considered that introns, present in DNA but excised during mRNA processing at conserved exon-intron boundary sequences[18,19], could allow for insertion of recombinase machinery directly into the gene without affecting the protein product. We first tested whether introns introduced into ChR2-eYFP would degrade protein functionality and if insertion of recombinase recognition sites into introns would impair splicing. We identified intron insertion sites that naturally mimic exonic splice sequences[18,19] near the middle of each ORF, such that individual exons would be unlikely to encode functional protein. We inserted two introns: intron B from cytomegalovirus IE1[20] ('intron 1'; 112bp) into ChR2 or intron 3 from mouse IgE[21] ('intron 2'; 82bp) into eYFP, either in native form or with addition of a *lox2722* ('+lox') site within regions not likely to function in splicing. We also created a construct containing both introns (Fig. 2a).

HEK293 cells transfected with any of these constructs expressed eYFP, suggesting proper splicing. cDNAs amplified from expressing cells and the source DNA were amplified by PCR using primer sets that spanned single introns (Fig. 2b) or both introns (Supplementary Fig. 4a). We noted variability in the size of the amplicon from the DNA template, whereas cDNA bands were uniform, further suggesting proper splicing. Upon sequencing, introns were absent from all cDNAs synthesized with primers spanning a single intron (Fig. 2c) or spanning both introns (except intron 1+lox, suggesting altered splicing in this modified intron; Supplementary Fig. 4b). To assay ChR2 function, we transfected neuronal cultures (Fig. 2d) and obtained patch-clamp recordings (Fig. 2e). Photocurrents were comparable to native ChR2-eYFP except for intron 2+lox photocurrents, which were larger (ChR2-eYFP: 1422±92 pA n=19; intron 2+lox: 2279±247 pA n=5, p<0.01). Neither exon fragment of ChR2 was able to generate photocurrents in isolation (Supplementary Fig. 5). Finally, to assay these constructs *in vivo*, we injected lentivirus into mouse prefrontal cortex (mPFC). All constructs expressed by 1 week, and sustained expression through at least 4 weeks (Fig. 2f, Supplementary Fig. 6). Together, these results indicate that short introns inserted into the ChR2-eYFP coding sequence are properly spliced, do not impair gene function, and enable addition of heterologous sequence to the reading frame.

We next sought to optimize intron 1 given impaired performance relative to intron 2. We identified differences between intron 1 and the consensus splice sequence[18,19]

(Supplementary Fig. 4c,d), systematically changed these to match the consensus, then analyzed splicing by RT-PCR (Supplementary Fig. 4e). The modified intron acceptor and intron 1+lox template gave mixed products (Supplementary Fig. 4f); one of these was the expected sequence, and the other was identical to ChR2 sequence 139 bp 5' to the expected splice site--likely revealing a cryptic splice site. Modification of either the exon or intron donor sequences produced a single, expected product, yet only the optimized intron donor sequence improved functional expression (ChR2-eYFP: 1316 ± 120 pA n=8, intron donor: 2219 ± 258 pA n=6, $p<0.05$, Fig. 2g, Supplemental Fig. 4g). We included this modification in all constructs using intron 1.

We next combined recombinases (Cre/Flp) and engineered introns, using the DIO strategy to independently manipulate ORF fragments. To target cells expressing Flp AND Cre (Fig. 3a), we inserted cDIO recombinase recognition cassettes in both introns and fDIO cassettes before and after the ChR2-eYFP coding sequence. Flp controlled direction of the entire ORF, while the second exon was additionally controlled by Cre (Fig. 3b,c). Here, we paired *loxN*[22] with *lox2722*, and *F3*[17] with *F5* (Supplementary Fig. 7), eliminating *LoxP* and *FRT* to prevent *trans* recombination[23] with legacy recognition sites in some transgenic animals. We configured the first and third exons in the antisense direction, reversing their order, and left the second in the sense direction (C_{on}/F_{on}-ChR2-eYFP; Fig. 3b, Supplementary Fig. 8a). Here, both recombinases are necessary to place all three exons into the sense configuration (Fig. 3c) and either recombinase alone cannot produce a complete reading frame for ChR2 or eYFP.

To assess splicing, we prepared cDNA from HEK293 cells co-transfected with Cre, Flp, and the C_{on}/F_{on}-ChR2-eYFP construct. A shift in band size between transfected DNA and cDNA was readily apparent (Fig. 3d); splicing was confirmed by sequencing (Fig. 3e). To assess functionality and specificity, we co-transfected cultured neurons or HEK293 cells with combinations of recombinases and C_{on}/F_{on}-ChR2-eYFP. eYFP expression was only observed in neurons co-expressing both Cre and Flp (Fig. 3f, Supplementary Fig. 8a), consistent with population flow-cytometry data in HEK293 cells (Fig. 3g). Neurons expressing Cre, Flp, and either ChR2-eYFP or C_{on}/F_{on}-ChR2-eYFP had comparable photocurrents (Fig. 3h) and light-evoked action potentials (Fig. 3i). To examine functional specificity, we patched cells blinded to ChR2 expression and based solely on recombinase expression (Supplementary Fig. 9a-c) and found photocurrents only in the triple-transfected condition (Supplementary Fig. 9d,e). Last, we assessed the impact of expressing non-active configurations of C_{on}/F_{on}-ChR2-eYFP (Supplementary Fig. 10a) and observed no deleterious effects on membrane properties (Supplementary Fig. 10b,c) or cell survival (Supplementary Fig. 10d). These data indicate that integrating multiple recombinases with heterologous introns is a viable strategy for intersectional expression dependent on Cre and Flp recombinases, with expression levels comparable to native, intron-free, non-recombinase-dependent counterparts. We term this system INTRSECT to describe its underlying principles: INTronic Recombinase Sites Enabling Combinatorial Targeting.

Function of Cre AND Flp dependent ChR2-eYFP *in vivo*

We next tested our intersectional expression strategy *in vivo*. We bred double-transgenic Parvalbumin (PV)-p2A-Cre;Somatostatin (SOM)-IRES-Flp mice and injected WT, -*Cre*, -*Flp*, or -*Cre;-Flp* mice with AAV-DJ-C_{on}/F_{on}-ChR2-eYFP driven by the human Synapsin (hSyn) or EF1α/HTLV (nEF) promoters in dorsal CA1 of hippocampus and mPFC. Rodent CA1 contains PV+/SOM-, PV-/SOM+, and PV+/SOM+ neurons[24], while mPFC lacks PV+/SOM+ cells[25]. With imaging maximized for sensitivity and positive cells defined by fluorescence above background, hippocampal expression was restricted to double-transgenic Cre/Flp animals, regardless of promoter (nEF: 6.5 cells per slice, n=37 slices from 4 animals; hSyn: 8.2 cells per slice, n=52 slices from 3 animals). WT, *PV-Cre*, and *SOM-Flp* animals displayed less than 1 cell per slice with fluorescence above background (Fig. 4), and no expression was observed in mPFC (not shown).

We next analyzed ChR2 functionality in slices prepared from *PV-p2a-Cre; SOM-IRES-Flp* animals injected with AAV-DJ-C_{on}/F_{on}-ChR2-eYFP driven by either hSyn or nEF. Using whole-cell patch-clamp with biocytin-filled pipettes (Fig. 4b), we found robust photocurrents that reliably drove action potentials (Fig. 4c,d). To characterize the identity of recorded cells, we stained for PV, SOM, and biocytin (Fig. 4e,f). Surprisingly, while all cells expressed SOM, only 8/27 were positive for PV and even these were weakly stained. Since some PV+/SOM+ cells are known to express only minimal PV[26,27], we additionally processed slices for morphological characterization[28]. Of cells that were recovered with identifiable processes within the slice (17/33), 14/17 were classified as OLM and the remaining 3/17 as bi-stratified (Fig. 4e,f); cell types known to express both PV and SOM[28].

To further characterize cells expressing C_{on}/F_{on}-ChR2-eYFP, we stained and imaged thin slices and obtained data consistent with slice patching: most C_{on}/F_{on}-ChR2-eYFP-expressing cells examined were immunohistochemically SOM(+)/PV(lo/-) but were only present in PV+/SOM+ animals (Fig. 4g-j). Recombinase transgene expression need not be restricted to cells readily identifiable by immunostaining[29]; we therefore crossed a separate *PV-IRES-Cre* mouse[30] with *SOM-IRES-Flp*. C_{on}/F_{on}-ChR2-eYFP expression was again limited to -*Cre;-Flp* double transgenic mice (5.2 cells/slice, n=33 slices), although with diminished fluorescence. Unlike *PV-p2a-Cre;SOM-IRES-Flp* mice, expression was largely restricted to immunohistochemically PV+/SOM+ positive cells (87% of cells PV+/SOM+, n=173 cells, Fig. 4k,l). Divergent expression of C_{on}/F_{on}-ChR2-eYFP in these double-transgenic mice is therefore likely driven by differences between the *PV-p2a-Cre* and *PV-IRES-Cre* transgenic lines themselves.

INTRSECT-based exclusion targeting: AND NOT

This modular intron and recombinase targeting strategy potentially facilitates additional expression logic through reorientation of exons within the standard backbone. We next sought to target cells expressing recombinase X AND NOT recombinase Y (C_{on}/F_{off}, C_{off}/F_{on}; Fig. 5a-*left*) by manipulating starting directions of exons (Fig. 5a-*right*, 5b, Supplementary Fig. 8b,c). We analyzed splicing in HEK293 cells and observed a large shift in cDNA amplicon size relative to transfected DNA (Fig. 5c) and confirmed successful splicing by sequencing (Fig. 5d). Neurons co-transfected with AND NOT constructs express

ChR2-eYFP in the presence of the single activating recombinase but not with both Cre and Flp (Figs. 5e,f, Supplementary Fig. 8b,c), consistent with flow cytometry population data (Fig. 5g). These constructs exhibited comparable peak photocurrents (Fig. 5h) that drove action potentials (Fig. 5i). We noted that C_{on}/F_{off}-CY had a depressed photocurrent vs. non-recombinase-dependent ChR2-YFP; unlike C_{on}/F_{on} or C_{off}/F_{on}, this construct contains a full recombinase cassette when active, with two ATG sequences in the spacer (Supplementary Fig. 11a), but scrambling these improved photocurrents (Supplementary Fig. 11b). We conclude from these results that multiple Boolean logical operations governing expression of a single genetically encoded tool may be achieved using INTRSECT through simple manipulation of a standard construct.

Projection targeting using multiple recombinases

We next combined fDIO and cDIO with projection-targeting strategies, in order to restrict expression to cells defined by both genetic identity and projection pattern. Targeting dopaminergic (DA) cells of the ventral tegmental area (VTA) projecting to nucleus accumbens (NAc) requires an intersectional strategy as neither all VTA-DA neurons (which project to numerous downstream areas) nor the entire VTA-NAc projection (which includes DA and non-DA cells[31]) describes this population. We confirmed that projection-based targeting alone was insufficient by injecting a retrograde virus, LT-HSV-mCherry-IRES-Cre (Figs. 6a, Supplementary Fig. 13a-d), into NAc, and AAV-cDIO-ChR2-eYFP into VTA of wild-type mice (Fig. 6b); only 48% of VTA eYFP+ cells were TH+ (Fig. 6c,d). To target DA VTA-NAc neurons, we injected LTHSV-lox-STOP-lox-mCherry-IRES-Flp into NAc of *TH-Cre* transgenic mice and AAV5-fDIO-ChR2-eYFP into VTA (Fig. 6e). Only VTA neurons that both express Cre (TH+) and are transduced by LT-HSV (NAc-projecting) should express Flp, and therefore activate fDIO-ChR2-eYFP. Indeed, 94% of VTA eYFP+ cells were clearly mCherry+ and 93% of VTA eYFP+ cells were TH+; 60% of mCh+/TH+ cells were eYFP+ (Fig. 6f,g). eYFP+ fibers were abundant in NAc (Fig. 6f), but absent in mPFC and basolateral amydala (BLA), as expected[32]. Occasional sparse eYFP+ fibers but no cell bodies were seen in negative controls lacking either Cre (WT mice; Supplementary Fig. 14a,b) or Flp (no LT-HSV injection; Supplementary Fig. 14c,d).

Extension of INTRSECT

Other applications, such as expression of XFPs alone, require adaptation of these multiple-recombinase tools to a single ORF; we achieved this by modifying the intron approach for use with eYFP (Supplementary Fig. 12). Here, the 5' and 3' halves of eYFP are under control of separate recombinases, with a single intron containing Cre and Flp DIO cassettes (Supplementary Fig. 12a,b). RT-PCR analysis using direction-specific primers suggested that eYFP sequence in C_{on}/F_{on}, C_{on}/F_{off}, and F_{on}/C_{off} variants was amplified from recombinase co-transfected HEK293 cells, but not source DNA (Supplementary Fig. 12c,d) and was verified by sequencing (Supplementary Fig. 12e). Flow cytometry indicated that eYFP was only expressed after co-transfection with appropriate recombinases, including AND NOT configurations at the analysis timepoint five days post-transfection (Supplementary Fig. 12f).

The modular design of INTRSECT opens the door to additional logical operations, including XOR, NAND, and others (Supplementary Fig. 15). As criteria differentiating cell types become more sophisticated, three-term Boolean logic may become desirable (e.g. a AND b AND c), heightening the value of identifying new recombinases; for example, Cre relatives VCre and SCre[33]. In preliminary work, we synthesized human codon-optimized VCre and SCre, created vcDIO- and scDIO-ChR2-eYFP vectors, and transfected these alongside Cre, Flp, and Dre in HEK293 cells (Fig. 6h). While scDIO/SCre did not function well, VCre induced robust eYFP expression in vcDIOChR2-eYFP without cross-activity (Fig. 6h).

Discussion

In defining the function of specific cell types, precise targeting has been a long-standing limitation, with expression of genetically-encoded tools generally constrained to populations defined by a single feature. To meet challenges of multi-feature targeting, we have developed and validated a flexible, modular, and generalized approach integrating multiple recombinases, intron engineering, and specialized viruses (INTRSECT). While separability of key recombinase pairings was seen here, contrary to previous reports of Cre/Dre independence[16] we observed Cre/*Rox* cross-reaction *in vitro* and *in vivo*. Cre and Dre are both phage-derived, with recognition sites sharing high homology in the 13bp palindromic region that determines recombinase pairing. Sites used here could contribute to this cross-reaction and other non-canonical sites may allow for their combined use. In any case, our results with Flp buttress independence from Cre, and establish this property for the first time with Dre.

The multiple-recombinase and viral methods used in INTRSECT may synergize with strategies for tracing connectivity across networks, such as engineered viruses[34]. It will be important to validate penetrance, specificity, and safety of viral tools in each system. In this regard, while we observed minimal inappropriate expression with our payload/virus combinations, AAVs can form end-to-end concatamers with payload deletion and rearrangement[35], a process that may induce expression in isolation[36] and could contribute (along with low TH expression) to the small population of TH-negative cells in projection-targeting experiments (Fig. 6f,g). Alternatively, read-through in HSV *lox-stop-lox* cassettes is possible, separate from INTRSECT constructs[7,10], and may be improved by alternative strategies (Supplementary Fig. 16a). However, absence of inappropriate expression in controls (Supplementary Fig. 14) suggests instead that targeting NAc-projecting cells may enrich for rare VTA TH- cells labeled by this transgenic line[8,32].

To create a single-AAV-based system capable of performing diverse Boolean logic on expression patterns, we built upon a substantial intron literature. Pioneering work adding heterologous introns to mammalian transgenes revealed that introns may function as independent units and that their addition to cDNAs can improve expression *in vitro*[20,37] and *in vivo*[38], consistent with our findings that introns inserted into ChR2-YFP are spliced and enhance photocurrents. The design and use of intron-containing fluorophores may facilitate integrating introns into genetic tools for increased expression. We relied on splice site descriptions[18,19] in optimizing INTRSECT constructs and found improved splicing correlated with increased photocurrents, emphasizing potential benefits of heterologous

introns. For future work requiring additional introns many options exist, although it may be sufficient to duplicate these two[39].

We tested the INTRSECT C_{on}/F_{on}-ChR2 variant by producing double-transgenic *PV-p2a-Cre;SOM-IRES-Flp* mice with populations of inhibitory neurons expressing only Cre (PV; axo-axonic and basket cells), only Flp (SOM; hippocampal projection neurons), or both Cre/Flp (PV;SOM O-LM and bi-stratified neurons)[24]. We observed robust expression within hippocampus of double-transgenic animals, but not single-transgenic or wild-type animals, nor in mPFC, consistent with PV and SOM expression patterns[25]. Additional experiments are indicated to characterize behavioral roles of these cells that are now targetable, and together with C_{on}/F_{off} and C_{off}/F_{on}, these reagents may be of immediate utility in studies of interneuron modulation of hippocampal function[27].

Validation of targeting in each system with multiple approaches is indicated. Here, we used IHC and morphologic analysis of targeted O-LM and bi-stratified hippocampal cells; electrophysiological and other properties may also be employed. Differences observed in targeted cell types between similar transgenic mouse lines underscores the importance of considering recombinase expression pattern in transgenic animals, including bicistronic knock-ins. Production of additional transgenic animals expressing Flp will augment options for targeting refined cell populations.

Individual components of the INTRSECT system, including viral, recombinase, and intron tools, may be separated or combined, as we have shown in targeting the NAc-projecting DA cells of the VTA. Beyond this example, cells in an "upstream" brain region that project to two different downstream regions could be targeted to either include or exclude neurons based on projection pattern (Supplementary Fig. 16a,b) and may be combined with transgenic recombinase mouse lines for additional specificity (Supplementary Fig. 16c). And while we have used ChR2-eYFP as a single targeted gene here, these tools also enable independent targeting and manipulation of multiple separately defined cell types within a single animal (Supplementary Fig. 16d). INTRSECT tools have a modular design, may be integrated with existing reagents and animals, and may enable diverse expression logic for genetically-encoded tools based on multiple genetic and/or connectivity factors.

METHODS

Statistical Analysis

All statistical tests were chosen based on normality of data and appropriateness of comparison to be analyzed by a particular approach. Data that were not normally distributed were either transformed to achieve normality, or analyzed with a test that does not assume normal distribution. Estimation of variance was performed by Bartlett's test for equal variance (for ANOVAs) or by an F test to compare variance (for unpaired t-tests). Variances were equal except when explicitly noted, below.

All error bars reported as s.e.m.

Fig. 2e. n = 19 for ChR2-eYFP group, n = 12 for intron 1 group, n = 5 for intron 1+lox group, n = 12 for intron 2 group, n = 5 for intron 2+lox group, n = 5 for intron 1+2 group. One-way Type I ANOVA detected significant difference between the means: $F_{5,52}$ = 2.856, p = 0.0237. ChR2 and intron 2+lox showed significant differences: p<0.01, Dunnett's multiple comparison test.

Fig. 2g. n = 8 for fSyn-ChR2-eYFP group, n = 5 for intron 1+lox group, n = 6 for iC4A group ("intron 1+lox optimized"). fSyn-ChR2-eYFP and iC4A showed significant differences: p<0.05, Dunnett's multiple comparison test.

Fig. 3h. n = 13 for ChR2 group, n = 7 for C_{on}/F_{on} group. Unpaired two-sided t-test showed no significant difference: p=0.1110.

Fig. 5h. n = 7 for fSyn-ChR2-eYFP group, n = 7 for C_{on}/F_{on} group, n = 7 for C_{on}/F_{off} group, n = 6 for F_{on}/C_{off} group. One-way Type I ANOVA detected significant difference between the means: $F_{3,23}$ = 3.553, p = 0.0301. No significant differences were detected by Dunnett's multiple comparison tests.

Molecular cloning

All single recombinase-dependent plasmids were constructed in an AAV-Ef1α backbone using the double-floxed inverted open-reading-frame (DIO) strategy described previously[7,8]. To construct Flp-dependent recombinant AAV vectors, a DNA cassette carrying two pairs of incompatible *FRT* sites (*FRT* and *F5*[17]) was synthesized and the ChR2-eYFP transgene was inserted between the two sites in the reverse orientation. The resulting cassette was cloned into a modified version of the pAAV2-MCS vector carrying the Ef1α promoter and the Woodchuck hepatitis virus posttranscriptional regulatory element (WPRE) to enhance expression. A similar strategy was used to construct the Dre-dependent plasmids, except since there was only one known *Rox* site[16], a novel *Rox* site ('*Rox2*') was designed (5' – aactttaaataatgtcgattatttaaagtta – 3').

Three constructs were used to deliver Cre into cells either *in vivo* or *in vitro*: AAV-Ef1α - Cre, AAV-Ef1α -Cre-p2A, AAV-EF1α -mCherry-IRES-Cre. The p2A peptide sequence was added where indicated as an immunostaining antigen. Similar constructs were used for Flp, Dre, VCre, and SCre. Dre, VCre, and SCre were human codon optimized and synthesized (DNA2.0, Mountain View, CA). All AAV vectors were tested for *in vitro* expression prior to viral production. Updated maps are available at optogenetics.org.

To create early multiple recombinase dependent constructs, we used two separate approaches to modifying cDIO-hChR2(H134R)-eYFP. First, by inverting the Ef1a promoter and flanking it with (5' of the promoter) *FRT* and *F5* in the forward direction and (3' of the promoter) *F5* and *FRT* in the reverse direction. This construct effectively has two tandem DIO cassettes: one that encompasses the promoter and one that encompasses the ORF; thus was named "Double Inverted Promoter/Double Inverted ORF (DIP/DIO)' AAV-fd DIP Ef1a-cd DIO hChR2 (H134R)-eYFP. Second, three other Cre and Flp dependent variants were created by leaving the promoter in the forward direction, but nesting Flp recognition sites such that the 5' forward direction sites were within one of the extracellular loops of

ChR2, while the 3' reverse direction sites were situated beyond the STOP codon. The portion of the ChR2 reading frame within the Flp recognition sites is initially in the forward direction, while the portion of the reading frame under control of only Cre is initially in the reverse direction. This second strategy retains a *F5* site within the coding frame of ChR2 in the active conformation that occurs after the recombination catalyzed by Cre and Flp.

Short introns identified by a literature search (Intron 1: CMV Towne Variant intron B[20] genbank M60321, Mouse IgE intron 3[21] genbank X01857.1) and derivatives were synthesized as oligos and inserted by overlapping PCR directly into the open reading frame of ChR2 or eYFP as indicated. Target sites for insertion were determined using two criteria: first, that the two bases 5' and the two bases 3' of the insertion site match the exonic 5' and 3' consensus splice site sequences, respectively; and second, that it would be unlikely that either fragment upstream or downstream of the reading frame translated in isolation would encode a functional protein. Splicing was tested *in silico* using NetGene2[40] (http://www.cbs.dtu.dk/services/NetGene2/). To test intron function, these modified ChR2-eYFP fusion genes were inserted into a lentiviral backbone driven by the human synapsin (hSyn) promoter between BamHI and EcoRI, scaled up and purified using endotoxin-free (Qiagen endotoxin-free MaxiPrep) or low endotoxin (Invitrogen MaxiCard) plasmid preparation kits for small batch lentiviral production.

To introduce recombinase recognition sites and enable directional control of individual exons, we first constructed a standard AAV backbone with a multiple cloning site downstream of either the hSyn or chimeric EF1 α/HTLV promoter consisting (from 5' to 3') of BamHI | AscI | SalI | SpeI | KpnI | NheI | XbaI | EcoRI through oligo ligation. We next identified likely donor, branch point, and acceptor regions in the intron by comparison to consensus sequences[18,19]. To ensure proper exon/exon joining, the donor and acceptor sequences for each intron were directly joined to their exonic partners, using overlapping PCR, without intervening restriction sites. To incorporate Flp control of all three exons, incompatible sites[17] *F3* and *F5* were separated by a short spacer sequence[8] and placed between BamHI and AscI in the sense direction and between XbaI and EcoRI in the antisense direction. To incorporate Cre control of the second exon, incompatible sites[22] *Lox2722* and *LoxN* were separated by the same spacer sequence and fused in the sense direction to the CMV (intron 1) bp and intronic sequence and in the antisense direction to the IgE (intron 2) bp and intronic sequence and placed between the SalI and SpeI and KpnI and NheI sites, respectively. *F3* and *LoxN* were chosen over *FRT* and *LoxP* to decrease the possibility of chromosomal translocation[23] in transgenic animals that harbor either of these sites in their genome as legacy sequence from antibiotic resistance cassettes used during animal production. With this standard acceptor vector, exon direction for each Boolean value was determined, correct restriction sites were placed on exons via PCR addition, and exons were ligated into the AAV acceptor vector. DNA was amplified as above for production of AAV. All constructs are freely available (www.optogenetics.org).

Construct variants for control experiments were built as follows: truncated ChR2 for exon function experiments were created by 1) fusing the 3' end of the exon 1 in-frame to eYFP, adding bases as necessary and 2) fusing the 3' end of the ChR2 portion of exon 2 to eYFP, adding an ATG start codon to the 5' end and bases as necessary to the 3' end to create a

functional reading frame. Constitutive blue fluorescent protein (BFP) was added to constructs for cell health experiments by 1) creating a BFP expression cassette consisting (5' to 3') of the hSyn promoter, BFP, and polyA tail. This was then cloned into a unique MluI site 5' of the hSyn promoter driving expression of cDIO-ChR2-eYFP, fDIO-ChR2-eYFP, or C_{on}/F_{on}-ChR2-eYFP such that it was independently expressed from the recombinase-dependent expression cassette.

Flow Cytometry

HEK 293FT cells (Invitrogen) were grown in 24-well tissue culture plates to 90% confluence and transfected in duplicate with 800 ng total DNA with Lipofectamine 2000 (Invitrogen) following the manufacturer protocol. Five days post-transfection, cells were removed by enzymatic dissociation (TrypLE, GIBCO), re-suspended in PBS, pelleted at 200 g × 5 min and re-suspended in 500 μL PBS supplemented with 1 μg/mL propidium iodide (PI; Sigma) then placed on ice under aluminum foil until analysis. Flow cytometry was completed on a Scanford analyzer at the Stanford Shared FACS Facility using settings optimized for Side Scatter (SS), Forward Scatter (FS), PI, and eYFP acquisition using positive (ChR2-eYFP), negative (empty transfection) and dead (heat-killed; 95 C × 3 min) conditions as controls. Live cell populations used in comparisons were isolated from debris and dead cells in post-hoc analysis by 1) negatively gating for PI+ cells, 2) positively gating for the high-density population in plotting FS vs. SS.

To unambiguously assess the expression of ChR2-eYFP in our samples, we subsampled each 30,000 point dataset into 100 independent datasets. The log-fluorescence (eYFP intensity) of each of these 100 subsets was then independently fit to a multi-component Gaussian mixture model that chose whether the dataset was best fit by one or more than one curve, using the Bayesian information criterion to generate an accurate statistical estimate of the distinct subpopulations best accounting for each set of observations.

Animals

Adult wild-type, male and female transgenic *Parvalbumin-IRES-Cre*[30] (Jax 008069), *Parvalbumin-2a-Cre*[29] (Jax 012358), *Tyrosine Hydroxylase-Cre* (EMMA 00254), and *Somatostatin-Flp* C57/BL6 mice were group housed up to four to a cage and kept on a reverse 12 hour light/dark cycle with *ad libitum* food and water. Experimental protocols were approved by Stanford University IACUC and meet guidelines of the National Institutes of Health guide for the Care and Use of Laboratory Animals.

Supplementary Material

Refer to Web version on PubMed Central for supplementary material.

Acknowledgments

REFERENCES

1. Crick FH. Thinking about the brain. Scientific American. 1979; 241:219–232. [PubMed: 115087]

2. Boyden ES, Zhang F, Bamberg E, Nagel G, Deisseroth K. Millisecond-timescale, genetically targeted optical control of neural activity. Nature neuroscience. 2005; 8:1263–1268.

3. Yizhar O, Fenno LE, Davidson TJ, Mogri M, Deisseroth K. Optogenetics in neural systems. Neuron. 2011; 71:9–34. [PubMed: 21745635]

4. Luo L, Callaway EM, Svoboda K. Genetic dissection of neural circuits. Neuron. 2008; 57:634–660. [PubMed: 18341986]

5. Zhang F. Fast optical neural circuit interrogation technology: development and applications. Larry Katz Memorial Lecture (Cold Spring Harbor Laboratory Meeting on Neuronal Circuits: From Structure to Function. 2008

6. Atasoy D, Aponte Y, Su HH, Sternson SM. A FLEX switch targets Channelrhodopsin-2 to multiple cell types for imaging and long-range circuit mapping. The Journal of neuroscience : the official journal of the Society for Neuroscience. 2008; 28:7025–7030. [PubMed: 18614669]

7. Sohal VS, Zhang F, Yizhar O, Deisseroth K. Parvalbumin neurons and gamma rhythms enhance cortical circuit performance. Nature. 2009; 459:698–702. [PubMed: 19396159]

8. Tsai HC, et al. Phasic firing in dopaminergic neurons is sufficient for behavioral conditioning. Science (New York, N.Y. 2009; 324:1080–1084.

9. Saunders A, Johnson CA, Sabatini BL. Novel recombinant adeno-associated viruses for Cre activated and inactivated transgene expression in neurons. Frontiers in neural circuits. 2012; 6:47. [PubMed: 22866029]

10. Kuhlman SJ, Huang ZJ. High-resolution labeling and functional manipulation of specific neuron types in mouse brain by Cre-activated viral gene expression. PloS one. 2008; 3:e2005. [PubMed: 18414675]

11. Awatramani R, Soriano P, Rodriguez C, Mai JJ, Dymecki SM. Cryptic boundaries in roof plate and choroid plexus identified by intersectional gene activation. Nature genetics. 2003; 35:70–75. [PubMed: 12923530]

12. Siuti P, Yazbek J, Lu TK. Synthetic circuits integrating logic and memory in living cells. Nature biotechnology. 2013; 31:448–452.

13. Marti T. Refolding of bacteriorhodopsin from expressed polypeptide fragments. The Journal of biological chemistry. 1998; 273:9312–9322. [PubMed: 9535926]

14. Schmitt C, Schultheis C, Husson SJ, Liewald JF, Gottschalk A. Specific Expression of Channelrhodopsin-2 in Single Neurons of Caenorhabditis elegans. PloS one. 2012; 7:e43164. [PubMed: 22952643]

15. Raymond CS, Soriano P. High-efficiency FLP and PhiC31 site-specific recombination in mammalian cells. PloS one. 2007; 2:e162. [PubMed: 17225864]

16. Sauer B, McDermott J. DNA recombination with a heterospecific Cre homolog identified from comparison of the pac-c1 regions of P1-related phages. Nucleic acids research. 2004; 32:6086–6095. [PubMed: 15550568]

17. Schlake T, Bode J. Use of mutated FLP recognition target (FRT) sites for the exchange of expression cassettes at defined chromosomal loci. Biochemistry. 1994; 33:12746–12751. [PubMed: 7947678]

18. Mount SM. A catalogue of splice junction sequences. Nucleic acids research. 1982; 10:459–472. [PubMed: 7063411]

19. Zhang MQ. Statistical features of human exons and their flanking regions. Human molecular genetics. 1998; 7:919–932. [PubMed: 9536098]

20. Chapman BS, Thayer RM, Vincent KA, Haigwood NL. Effect of intron A from human cytomegalovirus (Towne) immediate-early gene on heterologous expression in mammalian cells. Nucleic acids research. 1991; 19:3979–3986. [PubMed: 1650459]

21. Ishida N, Ueda S, Hayashida H, Miyata T, Honjo T. The nucleotide sequence of the mouse immunoglobulin epsilon gene: comparison with the human epsilon gene sequence. The EMBO journal. 1982; 1:1117–1123. [PubMed: 6329728]

22. Livet J, et al. Transgenic strategies for combinatorial expression of fluorescent proteins in the nervous system. Nature. 2007; 450:56–62. [PubMed: 17972876]

23. Zong H, Espinosa JS, Su HH, Muzumdar MD, Luo L. Mosaic analysis with double markers in mice. Cell. 2005; 121:479–492. [PubMed: 15882628]

24. Somogyi P, Klausberger T. Defined types of cortical interneurone structure space and spike timing in the hippocampus. The Journal of physiology. 2005; 562:9–26. [PubMed: 15539390]

25. Kawaguchi Y, Kubota Y. GABAergic cell subtypes and their synaptic connections in rat frontal cortex. Cereb Cortex. 1997; 7:476–486. [PubMed: 9276173]

26. Ferraguti F, et al. Immunolocalization of metabotropic glutamate receptor 1alpha (mGluR1alpha) in distinct classes of interneuron in the CA1 region of the rat hippocampus. Hippocampus. 2004; 14:193–215. [PubMed: 15098725]

27. Klausberger T, et al. Brain-state- and cell-type-specific firing of hippocampal interneurons in vivo. Nature. 2003; 421:844–848. [PubMed: 12594513]

28. Klausberger T. GABAergic interneurons targeting dendrites of pyramidal cells in the CA1 area of the hippocampus. The European journal of neuroscience. 2009; 30:947–957. [PubMed: 19735288]

29. Madisen L, et al. A robust and high-throughput Cre reporting and characterization system for the whole mouse brain. Nature neuroscience. 2010; 13:133–140.

30. Hippenmeyer S, et al. A developmental switch in the response of DRG neurons to ETS transcription factor signaling. PLoS biology. 2005; 3:e159. [PubMed: 15836427]

31. Van Bockstaele EJ, Pickel VM. GABA-containing neurons in the ventral tegmental area project to the nucleus accumbens in rat brain. Brain research. 1995; 682:215–221. [PubMed: 7552315]

32. Stamatakis AM, et al. A unique population of ventral tegmental area neurons inhibits the lateral habenula to promote reward. Neuron. 2013; 80:1039–1053. [PubMed: 24267654]

33. Suzuki E, Nakayama M. Cre/VloxP and SCre/SloxP: new site-specific recombination systems for genome engineering. Nucleic acids research. 2011; 39:e49. [PubMed: 21288882]

34. Wickersham IR, et al. Monosynaptic restriction of transsynaptic tracing from single, genetically targeted neurons. Neuron. 2007; 53:639–647. [PubMed: 17329205]

35. Yang J, et al. Concatamerization of adeno-associated virus circular genomes occurs through intermolecular recombination. Journal of virology. 1999; 73:9468–9477. [PubMed: 10516055]

36. Nakai H, Storm TA, Kay MA. Increasing the size of rAAV-mediated expression cassettes in vivo by intermolecular joining of two complementary vectors. Nature biotechnology. 2000; 18:527–532.

37. Buchman AR, Berg P. Comparison of intron-dependent and intron-independent gene expression. Molecular and cellular biology. 1988; 8:4395–4405. [PubMed: 3185553]

38. Palmiter RD, Sandgren EP, Avarbock MR, Allen DD, Brinster RL. Heterologous introns can enhance expression of transgenes in mice. Proceedings of the National Academy of Sciences of the United States of America. 1991; 88:478–482. [PubMed: 1988947]

39. Reed R, Maniatis T. A role for exon sequences and splice-site proximity in splice-site selection. Cell. 1986; 46:681–690. [PubMed: 2427200]

40. Brunak S, Engelbrecht J, Knudsen S. Prediction of human mRNA donor and acceptor sites from the DNA sequence. Journal of molecular biology. 1991; 220:49–65. [PubMed: 2067018]
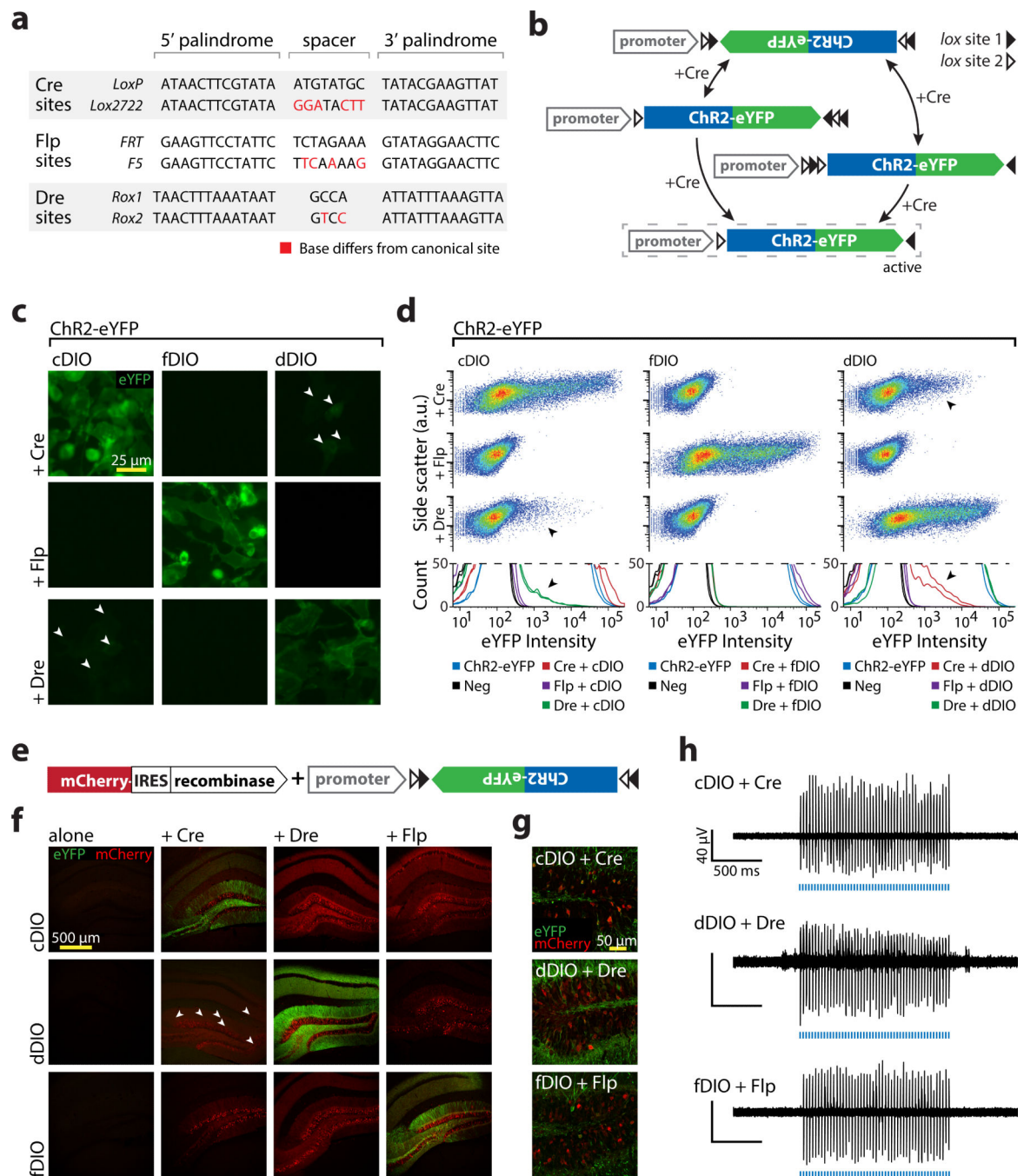
**Figure 1. Diversifying recombinase targeting strategies**

a) Recombinase recognition site sequences used in Double Inverted Open reading frame (DIO) constructs. **b)** Schematic of recombinase-mediated expression of a DIO construct. The ORF is initially inverted relative to the promoter and flanked by two sets of incompatible recombinase recognition sites. The recombinase first inverts the gene of interest into the forward orientation then either returns the gene to the starting position or excises two recognition sites and locks the gene in the forward orientation. **c)** HEK293 cells transfected with recombinase/DIO combinations. Arrowheads indicate Cre/Dre cross-

reactivity. **d)** Flow cytometry analysis of cells from **c**. Dot plot (*top*) and histograms (*bottom*) include biological replicates and controls. DIOs in isolation were comparable to negative control (92%-98% of samples fit by single curve) and were robustly expressed when paired with correct recombinase (99%-100% of samples fit by multiple curves). Cross-reaction was noted between Cre and Dre (multiple populations fit in 78% and 92% for cDIO + Dre, 100% for dDIO + Cre; arrowheads), but not Flp (96%-100% of samples fit with single curve). **e)** Viruses used in **f-h**. Each DIO was injected into mouse hippocampus alone or with a recombinase. **f,g)** Recombinase/DIO expression *in vivo* at low (**f**) or high (**g**) magnification. No leak was visible in absence of recombinase, and correct recombinase/DIO pairs were expressed well. Sparse expression was seen with dDIO + Cre (arrowheads; Supplementary Fig. 1; imaging individually optimized). **h**) *In vivo* optrode recordings in animals co-injected with proper recombinase/DIO pairings.
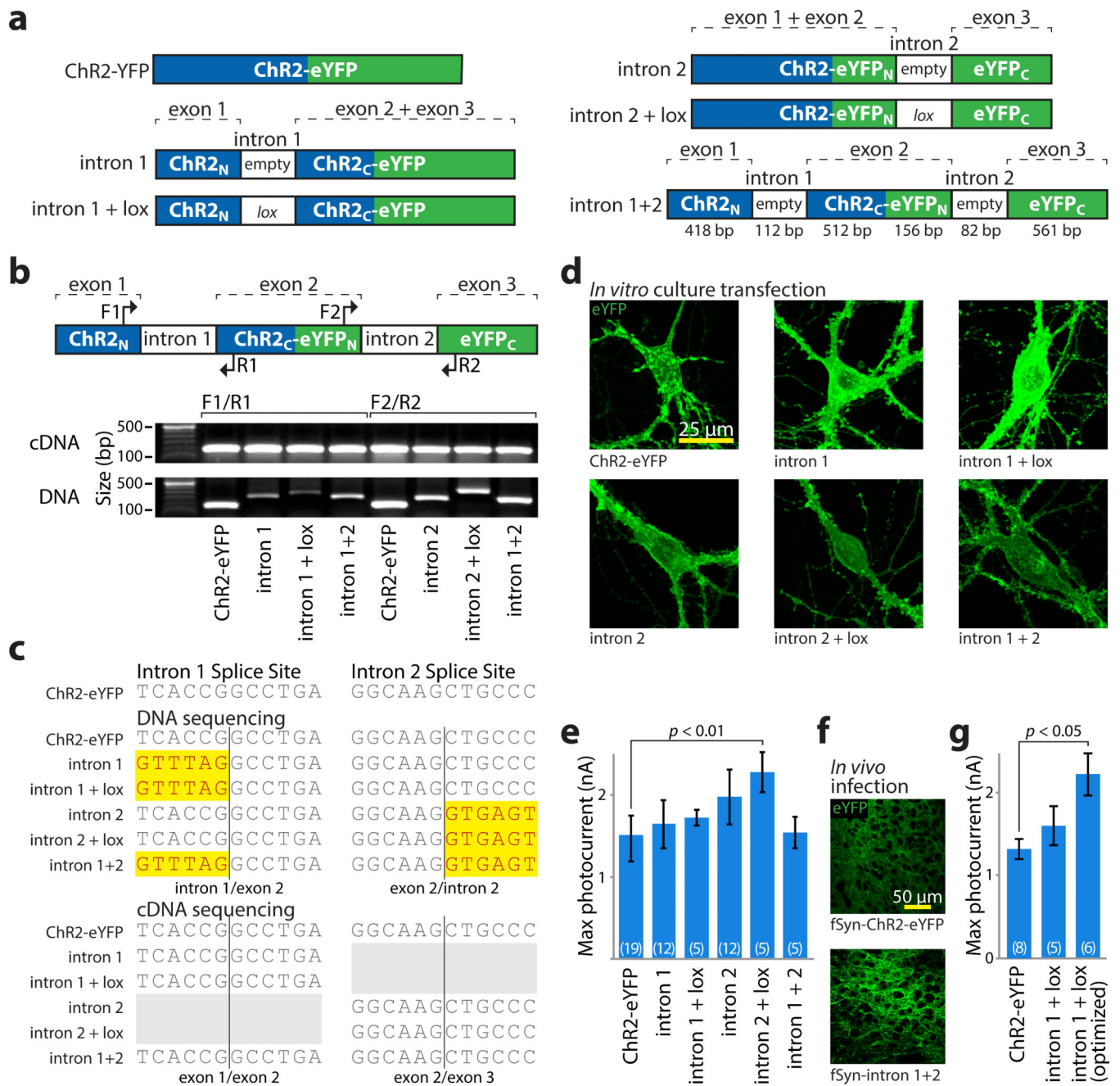
Figure 2. Intron engineering and validation for INTRSECT

a) Schematic of constructs and nomenclature. 'empty' denotes native introns, '*lox*' indicates addition of *lox2722* site (see methods). **b)** cDNA was prepared from mRNA of HEK293 cells transfected with indicated constructs. Source DNA and cDNA were amplified by PCR with primers (*top*) in either exons 1 and 2 ('F1/R1') or exons 2 and 3 ('F2/R2') and separated by gel electrophoresis (*bottom*). Note that non-spliced DNA bands containing introns vary in size, while cDNA bands from spliced mRNA are uniform. **c)** Sequence of DNA isolated from bands in **b**, with uniform removal of intron sequence with these primer sets. **d)** Images of eYFP expression in primary neuronal cultures transfected with indicated

constructs. **e)** Whole cell photocurrents from primary neurons transfected with intron constructs (ChR2-eYFP: 1422.1±91.7 pA n=19, intron 1: 1590.5±186.7 pA n=12, intron 1 + lox: 1721.7±97.8 pA n=5, intron 2: 1861.6±159.1 pA n=12, intron 2 + lox: 2279.1±246.9 pA n=5, intron 1 + intron 2: 1539.5±188.8 pA n=5, p<0.01 Dunnett's multiple comparison tests ChR2-eYFP vs. intron 2 + lox). All error bars s.e.m. **f)** Representative images of eYFP expression in medial prefrontal cortex of mouse brain at 2 weeks post-infection timepoint with lentivirus made from indicated constructs (see Supplementary Figure 6 for full dataset). **g)** Whole cell photocurrents illustrating increased peak photocurrent activity after intron 1 optimization (ChR2-eYFP: 1316±120 pA n=8, intron 1 + lox2722: 1603±236 pA n=5, intron donor: 2219±258 pA n=6, p<0.05 Dunnett's multiple comparison tests, ChR2-eYFP vs. intron donor; see Supplementary Figure 4).
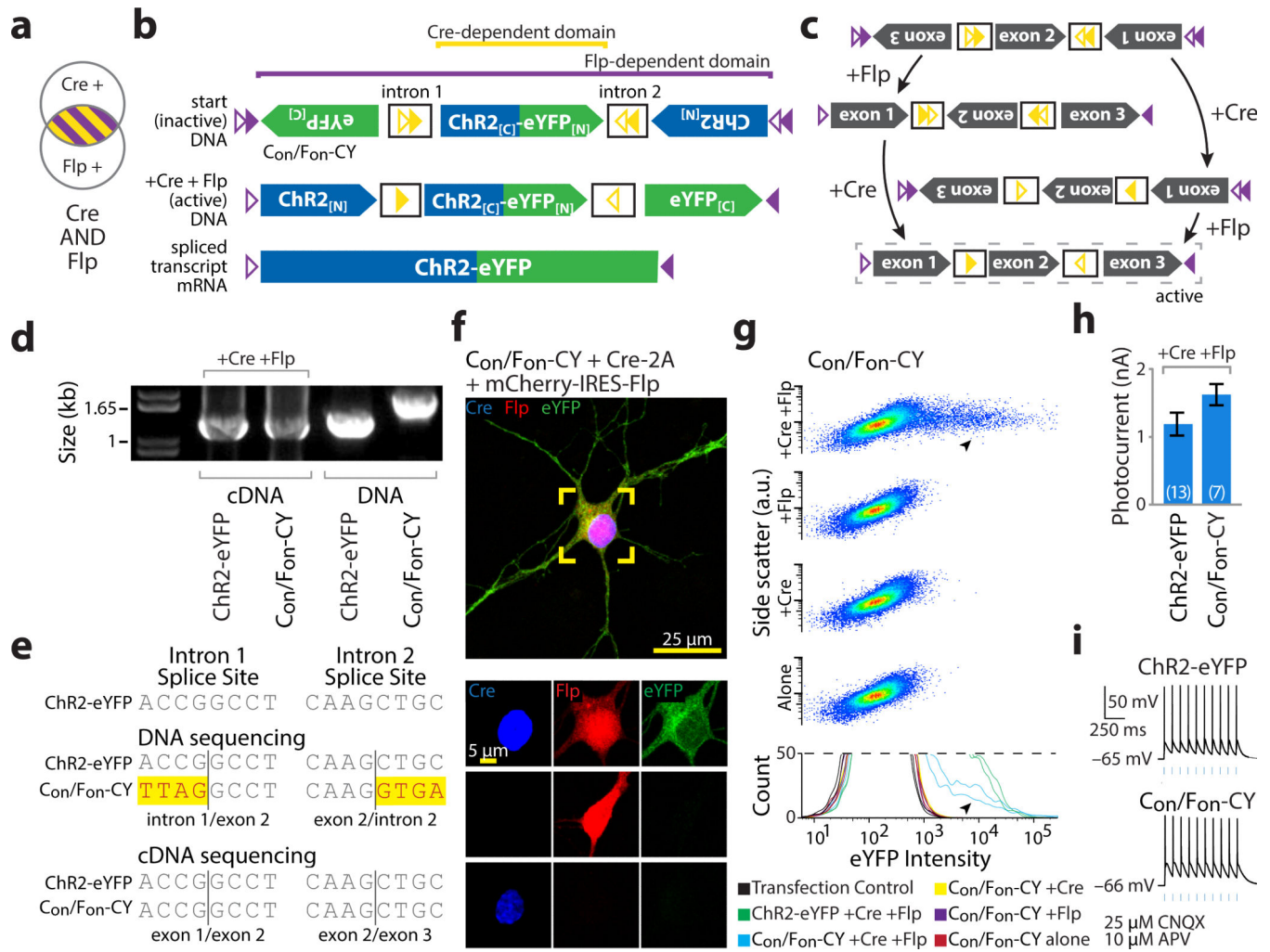
Figure 3. INTRSECT: diverse recombinases with engineered introns enable intersectional targeting *in vitro*

a,b) Schematics representing (**a**) cells targeted by nesting Cre-dependent directional control of a central exon and Flp-dependent directional control of all three exons (**b** *top*), such that both recombinases are necessary for all exons of the construct (C_{on}/F_{on}-ChR2-eYFP) to be in the sense direction (**b** *bottom*). **c)** Intermediate configurations in the activation of C_{on}/F_{on}-ChR2-eYFP. **d)** cDNA prepared from HEK293 cells transfected with indicated constructs and recombinases and source DNA were amplified using primers in exons 1 and 3 and separated by gel electrophoresis. Note size difference in bands from intron-containing DNA and uniformity of cDNA bands, suggesting successful splicing. **e)** Sequences of bands from **d.** Yellow denotes difference from ChR2-eYFP map sequence, representing intron sequence. **f)** eYFP is only expressed in the presence of both Cre and Flp in cultured neurons transfected with C_{on}/F_{on}-ChR2-eYFP (green), Cre (blue), and Flp (red) (see Supplementary Fig. 8). **g)** Flow cytometry dot plot (*top*) and biological replicate histograms (*bottom*) of HEK293 cells transfected with indicated recombinase/construct combinations. YFP expression is only seen with C_{on}/F_{on}-ChR2-eYFP and both Cre and Flp (arrowheads; 100% of norecombinase, Cre-alone, and Flp-alone transfections fit by a single curve, 100% of

Cre/Flp co-transfections fit by multiple curves). **h,i)** Whole cell photocurrents (**h**) and action potentials (**i**) recorded from primary neurons transfected with ChR2-eYFP or C_{on}/F_{on}-ChR2-eYFP and Cre/Flp indicate robust ChR2 function comparable to native ChR2 (ChR2-eYFP: 1120 ± 187 pA, n=6, C_{on}/F_{on}-ChR2-YFP: 1621 ± 157 pA, n=7 p=0.3542: two-sided unpaired t-test); all error bars s.e.m.
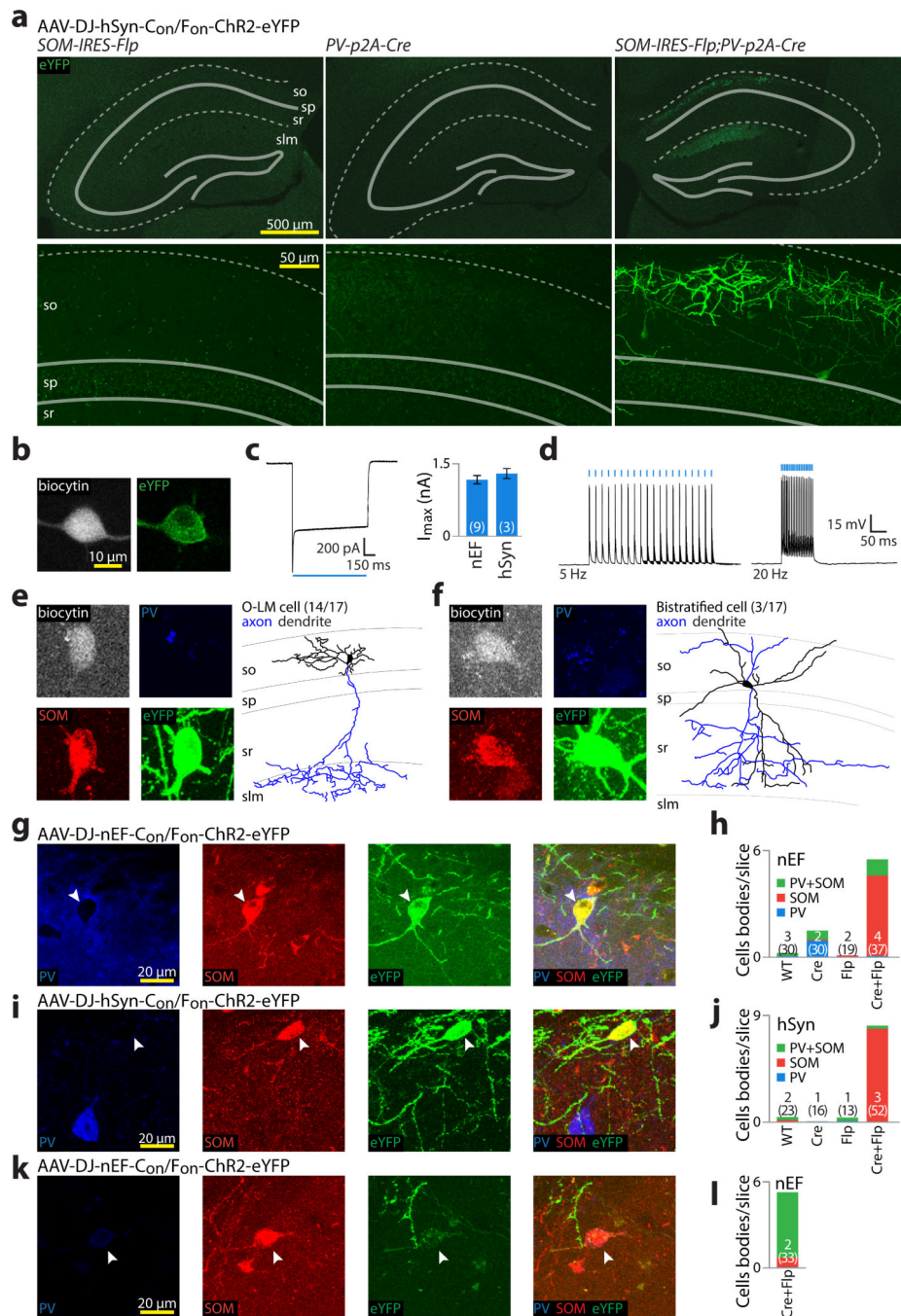
Figure 4. INTRSECT specificity and functionality *in vivo*
a) Hippocampal slices prepared four weeks after *SOM-IRES-Flp* (*left*), *PV-2a-Cre* (*middle*), or *PV-2a-Cre;SOM-IRES-Flp* (*right*) animals were injected with AAV-DJ-C_{on}/F_{on}-ChR2-eYFP. Expression was only seen in double transgenic animals, with eYFP+ cell bodies limited to the superficial hippocampus (so: stratum oriens; sp: stratum pyramidale; sr: stratum radiatum; slm: stratum lacunosum-moleculare). **b-d)** eYFP+ cells in *PV-2a-Cre;SOM-IRES-Flp* animals expressing C_{on}/F_{on}-ChR2-eYFP were patched with biocytin filled pipettes (**b**), and assayed for peak photocurrent (**c**) and action potentials (**d**). **e-f)** After

patching, slices were stained for biocytin (grey), PV (blue), and SOM (red) for identification (**e,f** *left*), followed by morphological reconstruction (**e,f** *right*). All error bars s.e.m. All identified neurons were either O-LM (**e**) or bi-stratified (**f**) and stained SOM(+), but apparently PV(lo/-) and were therefore identified largely based on their morphology. **g-j**) To characterize more thoroughly the cells targeted in *PV-2a-Cre;SOM-IRES-Flp* animals by C_{on}/F_{on}-ChR2-eYFP, slices from wild type, *PV-2a-Cre*, *SOM-IRES-Flp*, and *PV-2a-Cre;SOM-IRES-Flp* animals injected with virus driven by either hSyn or nEF were stained for SOM and PV. YFP+ cells driven by both nEF (**g,h**) and hSyn (**i,j**) stained SOM(+), but PV(-) (**g,i;** *arrowheads*). Imaging settings optimized for sensitivity detected negligible inappropriate expression in all but a single of 11 control animals, while double transgenic animals had high levels of expression (**h,j**). **k,l**) To examine the contribution of transgenic lines on virus expression, nEF-C_{on}/F_{on}-ChR2-eYFP was injected into dorsal CA1 of *PV-IRES-Cre;SOM-IRES-Flp* mice; despite relatively weak expression (**k**), YFP was almost completely restricted to cells co-expressing PV and SOM (**k,l;** *arrowhead*).
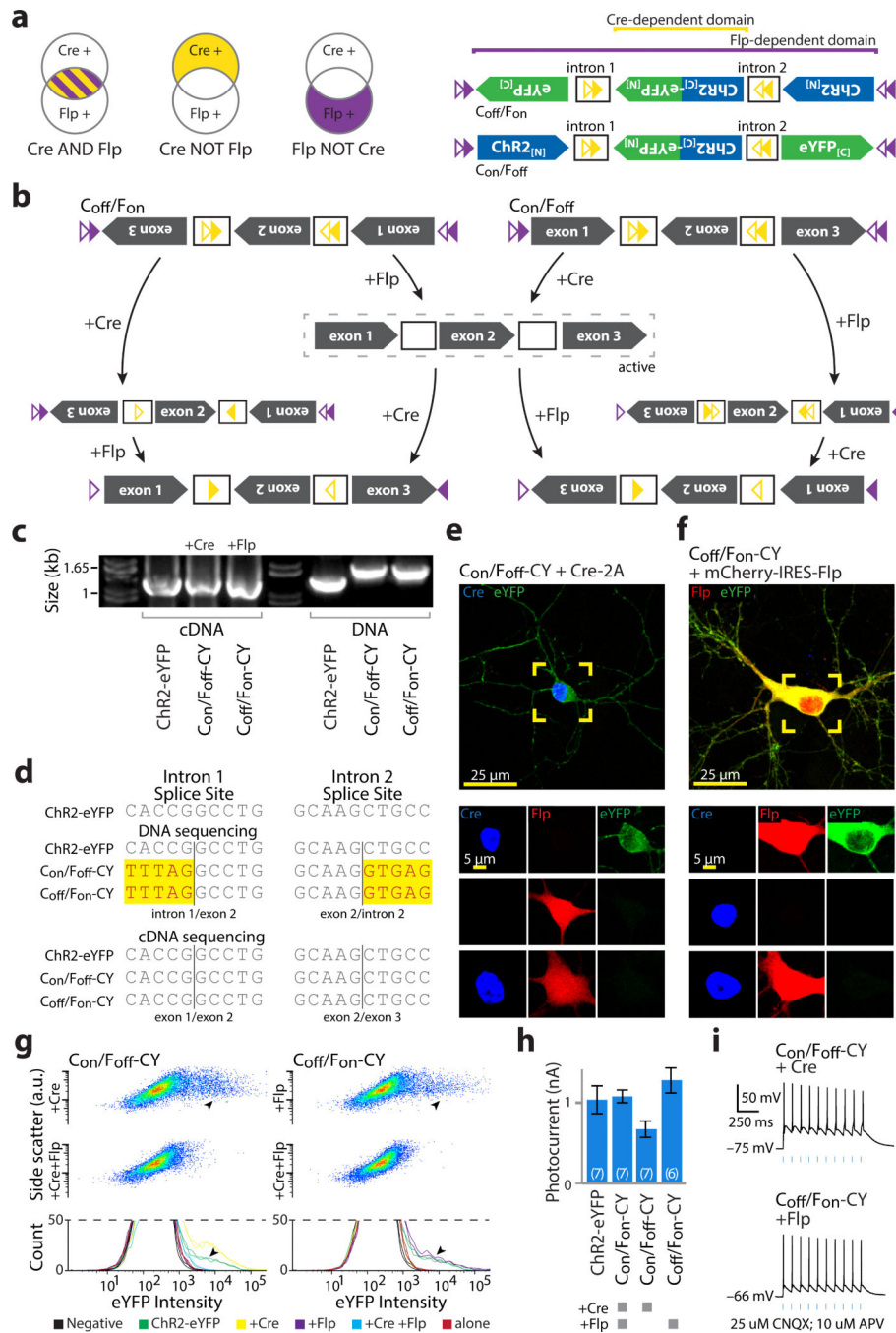
Figure 5. Exclusion logic using INTRSECT

a) Schematics representing target populations of cells expressing Cre and Flp (*left*) by nesting Cre-dependent directional control of a central exon and Flp-dependent directional control of all three exons (*right*). **b)** Intermediate states driven by Cre and Flp on constructs dependent on the exclusive presence of a single recombinase for functional expression (dashed box). **c)** cDNA prepared from mRNA of HEK293 cells transfected with indicated constructs and recombinases and source DNA were amplified by PCR with primers in exons 1 and 3 and separated by gel electrophoresis. Note variation in the size of bands from intron-

containing DNA template and uniformity of cDNA bands, suggesting successful splicing. **d)** Sequences of bands from **b.** Yellow denotes differences from ChR2-eYFP map sequence, representing intron sequence. **e,f) e**YFP is only expressed in cultured neurons transfected with combinations of Cre (blue), Flp (red), and C_{on}/F_{off} (**e;** green) or C_{off}/F_{on} (**f;** green) in the exclusive presence of Cre or Flp. **g)** Dot exemplar (*top*) and replicate histograms (*bottom*) of flow cytometry analysis of HEK293 cells transfected with indicated recombinase/construct combinations indicates expression in the presence of a single recombinase (arrowheads) that is extinguished when both recombinases are present, which was confirmed by Gaussian mixture model analysis (multiple populations fit in 85%-96% of matched single-recombinase transfections, single population fit in 94%-99% of double-recombinase transfections). **h,i)** Whole cell photocurrents (**h**) and action potentials (**i**) recorded from primary neurons transfected with ChR2-eYFP or C_{on}/F_{on}, C_{on}/F_{off}, C_{off}/F_{on}-ChR2-eYFP and Cre and Flp as indicated. All error bars s.e.m.
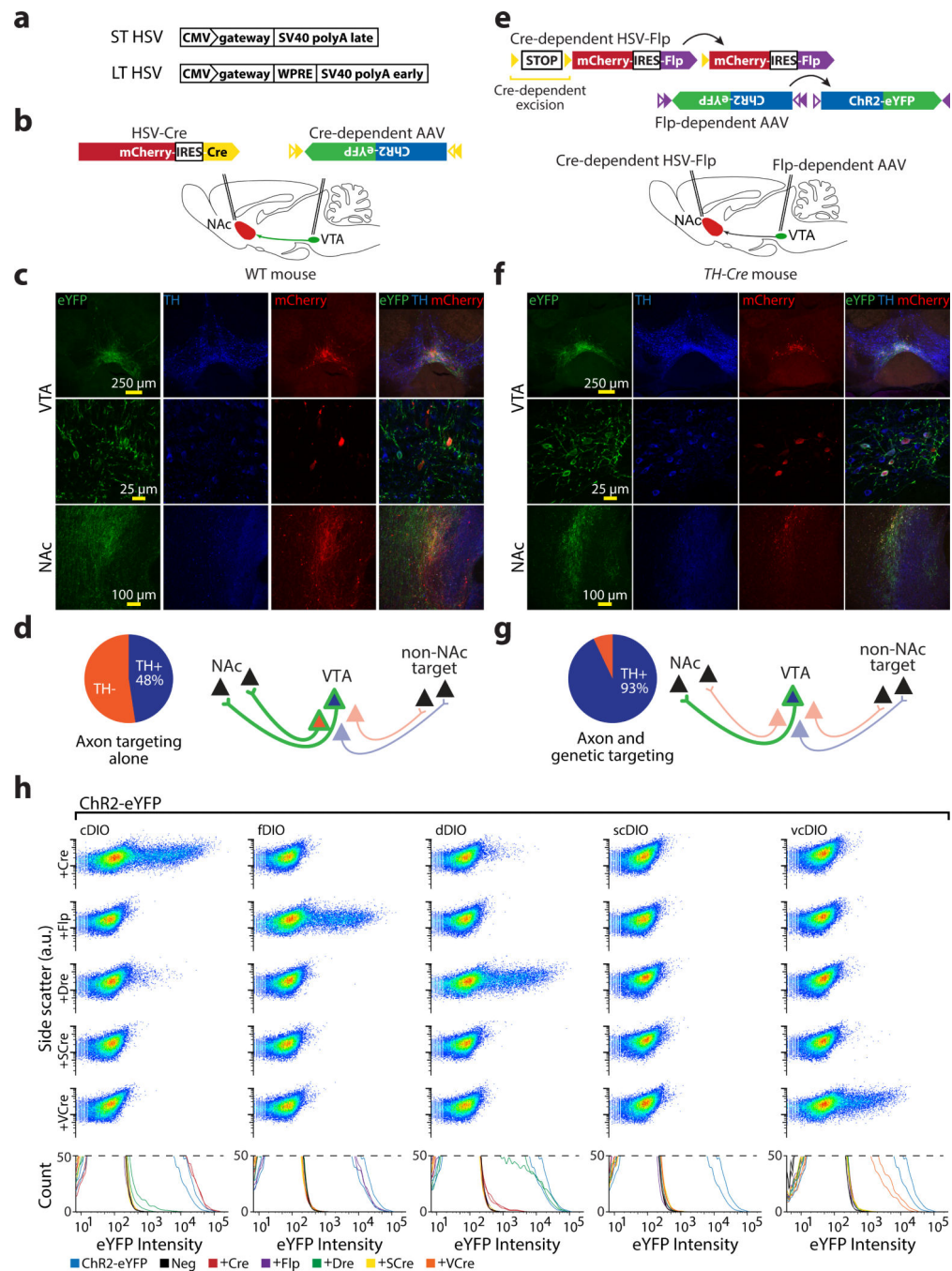
Figure 6. Combinatorial targeting with multiplexed recombinases: beyond genetic properties
a) Comparison of short-term (ST-HSV) and optimized long-term (LT-HSV) backbones. **b**)
Projection-based targeting of the NAc-projecting VTA cells in a wild-type mouse.
Retrograde LT-HSV-mCherry-IRES-Cre was injected into the NAc, while AAV-cDIO-
ChR2-eYFP was injected into the VTA. **c,d**) *In vivo* expression pattern observed with
projection-based targeting. Robust eYFP expression was observed within VTA, co-localized
with TH in only 48% (69/145) of cells, indicating expression in both dopaminergic and non-
dopaminergic VTA-NAc projection neurons. eYFP+ fibers were seen within the NAc. **e**)

Schematic illustrating strategy for combination projection/genetic targeting of the NAc-projecting TH+ VTA cells in a *TH-IRES-Cr*e mouse. Cre-dependent Flp was packaged into a retrograde LT-HSV and injected into the NAc, while AAV-fDIO-ChR2-eYFP was injected into the VTA. **f,g**) *In vivo* expression pattern observed with combination projection/genetic based targeting. eYFP expression in the VTA was highly co-localized with TH staining (145/156 cells), indicating restriction of expression to dopaminergic VTA-NAc projection neurons. eYFP+ fibers were seen within the NAc. **h)** Dot exemplar (*top*) and replicate histograms (*bottom*) of flow cytometry analysis of HEK293 cells transfected with indicated recombinase-dependent ChR2-eYFP constructs and recombinases indicate that codon-optimized VCre is able to activate vcDIO in mammalian cells (100% of samples fit to multiple curves) and does not cross-activate cDIO or fDIO (93%-98% of off-target DIOs fit with single curve). Moreover vcDIO is not activated by Cre and Flp. Note again cross-reaction between Cre/dDIO and Dre/cDIO. Specificity was quantitatively verified by Gaussian mixture model fits/analysis.